Arabian Journal of Chemistry (2019) **12**, 1479–1486

King Saud University

Arabian Journal of Chemistry

www.ksu.edu.sa
www.sciencedirect.com

ORIGINAL ARTICLE

Preparation of superhydrophobic nanocalcite crystals using Box–Behnken design

Said M. El-Sheikh [a], Ahmed Barhoum [b,*], Samya El-Sherbiny [c], Fatma Morsy [c], Ayman Abdel-Hamid El-Midany [d], Hubert Rahier [b]

[a] *Nanostructured Materials Division, Advanced Materials Department, CMRDI, P.O. Box 87, Helwan 11421, Cairo, Egypt*
[b] *Department of Materials and Chemistry, Vrije Universiteit Brussel, Pleinlaan 2, 1050 Brussels, Belgium*
[c] *Applied Chemistry, Chemistry Department, Faculty of Science, Helwan University, 11795 Helwan, Egypt*
[d] *Faculty of Engineering, Mining, Petroleum and Metallurgical Department, Cairo University, Giza, Egypt*

Received 27 August 2014; accepted 3 November 2014
Available online 10 November 2014

KEYWORDS

Nanocalcite crystals;
Bubbling carbonation;
Box–Behnken design;
Surface modification;
Hydrophobicity;
Particle surface charge

Abstract Superhydrophobic nanocalcite crystals were prepared via an adjusted aqueous reaction of CaO, CO_2 gas and sodium oleate. Box–Behnken design was used to optimize the preparation parameters such as CaO concentration, CO_2 gas flow rate and surfactant concentration. The results revealed that the produced $CaCO_3$ is indexed to the calcite phase. The crystallite size, particle size, morphology, hydrophobicity and surface charge of $CaCO_3$ are significantly affected by changing the preparation parameters. The addition of sodium oleate helps in reducing the crystallite size from 101 nm to 48 nm, reducing the particle size from 1.5 μm length scalenohedral particles to 40 nm rhombohedral particles and modifying the properties of pure $CaCO_3$ from highly hydrophilic to superhydrophobic.

1. Introduction

Calcium carbonate particles have a large number of industrial applications due to their beneficial properties such as high porosity, low cost, lack of toxicity and biocompatibility towards body fluids. Consequently, there has been significant research to deliver simple techniques for synthesizing $CaCO_3$ particles at specific sizes, polymorphs and morphologies (Rodriguez-Blanco et al., 2011; Wu et al., 2007). Calcium carbonate is an extremely important material, both in the fundamental research and industry. It has been used as a filler material for plastics, paints, papers and coats and can be moulded by organisms into complex and beautiful shapes as in bones, teeth and shells. $CaCO_3$ can exist in mainly four polymorphs: calcite, vaterite, aragonite and amorphous calcium carbonate (ACC), out of which calcite is the most thermodynamically stable phase. The ACC phase is unstable and relatively short-lived and acts as a seed for crystal growth of the other polymorphs (Ihli et al., 2014; El-Sheikh et al., 2013).

* Corresponding author.
E-mail address: ahmed.abdelrasoul@vub.ac.be (A. Barhoum).
Peer review under responsibility of King Saud University.

Production and hosting by Elsevier

http://dx.doi.org/10.1016/j.arabjc.2014.11.003
1878-5352

Several research efforts have shown that nano $CaCO_3$ has interesting properties over the micro $CaCO_3$ particles (1–10 μm). For example, studies on effects of $CaCO_3$ nanofillers in sealants and polymers (Avella et al., 2001; Di Lorenzo et al., 2002; Liang et al., 2013; Barhoum et al., 2014) have indicated that nano $CaCO_3$ ($\leqslant$100 nm) is particularly useful for filling sealants and increasing the stiffness of both the homo and copolymers than micro $CaCO_3$. However, the aggregation of nano $CaCO_3$, which is often detected in particulate filled polymers, can result in a number of problems, like deteriorated thermal and mechanical properties. The hydrophilic nature and tendency towards aggregation of nano $CaCO_3$ make it hardly usable in polymer matrixes and very difficult to be used at industrial scale production (Brecevic and Kralj, 2007). The recent research on surface modification of nanosize $CaCO_3$ with hydrophobic species such as fatty acids leads to a great expansion in its applications (Ukrainczyk et al., 2009). Such surfactants can bind with certain crystal planes during crystal growth, thereby changing the particle morphology and surface properties from hydrophilic to hydrophobic (Lanzon et al., 2011; Wang et al., 2010; Sheng et al., 2006). Calcium carbonate can be produced either by: (1) wet carbonation route, through a double decomposition reaction, wherein aqueous $CaCl_2$ and Na_2CO_3, or $CaCl_2$ and $(NH_4)_2CO_3$, or $Ca(NO_3)_2$ and Na_2CO_3 are combined in an equal molar ratio; or (2) the bubbling carbonation route, in which CO_2 gas is bubbled through an aqueous slurry of $Ca(OH)_2$ (Barhoum et al., 2014; Ihli et al., 2014; Ukrainczyk et al., 2007; Reeder et al., 2013). The bubbling carbonation route is industrially used because of the availability of its raw materials, high yield as well as simplicity and low cost of production (Tomioka et al., 2012; García Carmona et al., 2003). The bubbling carbonation is preferable in terms of environment preservation and the effective use of mineral resources.

According to the literature, little is known about the influence of the CaO concentration, CO_2 flow rate and surfactant on the characteristics of $CaCO_3$ particles at the same time. The effect of these parameters on the crystallite size of $CaCO_3$ particles has not been well-addressed yet. The goal of the present study is to prepare superhydrophobic $CaCO_3$ crystals using the bubbling carbonation technique and investigate the effects of the preparation parameters on the polymorph, crystallite/particle size, morphology, and particle surface characteristics of $CaCO_3$. Box–Behnken statistical experimental design was used to optimize the factors affecting the preparation of $CaCO_3$, such as CaO concentration, CO_2 flow rate and surfactant concentration. A fatty acid surfactant (sodium oleate) was used during the preparation to study its effect on crystal growth and to modify the hydrophobicity of $CaCO_3$.

2. Experimental

2.1. Materials

Analytical grade sodium oleate ($C_{18}H_{33}NaO_2$, 82 + % oleic acid, Sigma), calcium oxide (CaO, 97 + % on dry substance, Acros Organics), carbon dioxide gas (CO_2 gas, 99 + %, Air Liquide) and monodistilled water were used to prepare $CaCO_3$ particles.

2.2. Method

To minimize the number of experiments, Box–Behnken design of experiments (Michaux et al., 2013; Zaky et al., 2008) was used to optimize the effects of CaO concentration, CO_2 flow rate and surfactant concentration. The design matrix of different runs, 15 experiments, as well as the levels of each factor are shown in Table 1. In practice, preparation of $CaCO_3$ was carried out in a polypropylene plastic flask. The required amount of CaO reagent was slaked in 400 mL monodistilled water containing sodium oleate, and then the obtained lime was cooled to 25 °C. After cooling, the pure CO_2 gas was blown into the lime milk from the bottom of the plastic bottle under vigorous stirring. The CO_2 gas flow was controlled by a flow metre. The pH value of the reaction solution was monitored online using a pH metre (Jenway 3305). The pH of the CaO slurry is about 14 due to dissolution of CaO forming OH^- ions and decreases upon bubbling CO_2 gas through the solution. When the pH value decreased from 14 to 9, the reaction was completed (Wen et al., 2010) and the CO_2 flow was stopped. The produced slurry was filtered and washed three times using 100 mL monodistilled water, filtered, and dried at 120 °C in an oven for 24 h to obtain $CaCO_3$ powder. According to Box–Behnken design, optimal conditions were estimated using a second order polynomial function by which a correlation between studied factors and response (crystallite size) was generated. The general form of this equation is:

$$E(y) = \beta_0 + \sum_{i=1}^{3}\beta_i x_i + \sum_{i=1}^{3}\sum_{j=1}^{3}\beta_{ij} x_i x_j + \sum_{i=1}^{3}\beta_{ii} x_i^2, \quad (1)$$

where y is an estimate of the response variable and x_is are the independent variables that are known for each experimental run. The parameters β_0, β_i, β_{ii} and β_{ij} are the regression parameters. Software package, Design-Expert 6.1, Stat-Ease, Inc., Minneapolis, USA, was used for the regression analysis of experimental data and to plot the response surface. Analysis of variance (ANOVA) was used to estimate the statistical parameters. The extent of fitting the experimental results to the polynomial model equation was expressed by the determination coefficient, R^2. F-test was used to estimate the significance of all terms in the polynomial equation within a 95% confidence interval.

2.3. Characterization

The polymorph and the average crystallite size of the prepared $CaCO_3$ were characterized using X-ray diffraction (XRD, Bruker AXS D8, Germany) with Cu-Kα (λ = 1.5406 Å) radiation. The crystallite size of $CaCO_3$ was determined from X-ray diffraction data using Debye–Scherrer formula:

$$d_{RX} = K\lambda/\beta\cos\theta, \quad (2)$$

where d_{RX} is the crystallite size, K = 0.9 is a correction factor to account for particle shapes. β is the full width at half maximum (FWHM) of the most intense diffraction peak, λ is the wave length of the Cu target, and θ is the Bragg angle.

The morphology information was investigated using a high resolution transmission electron microscope (TEM, Jeol, JEM-2010, Japan). Bonding structures were analysed using

Table 1 Coded factor levels for the preparation of $CaCO_3$.

Run no.	CaO conc.	CO_2 flow rate	Surf. conc.
R1	−1	−1	0
R2	+1	−1	0
R3	−1	+1	0
R4	+1	+1	0
R5	−1	0	−1
R6	+1	0	−1
R7	−1	0	+1
R8	+1	0	+1
R9	0	−1	−1
R10	0	+1	−1
R11	0	−1	+1
R12	0	+1	+1
R13	0	0	0
R14	0	0	0
R15	0	0	0
Factors and levels for experimental design using Box–Behnken method			
Variables	−1	0	+1
CaO conc. (M)	0.1	0.55	1
CO_2 flow rate (ml min^{-1})	100	300	500
Surf. conc. (wt SO/wt $CaCO_3$)	0	2	4

Fourier transform infrared spectrometer (FT-IR-460plus, JASCO model 6100, Japan).

The water contact angle (WCA) was measured with a Kruss DSA-100 contact angle analyser. Measurements were performed on the prepared powders compressed into discs using 5 μL water droplet volume and the contact angle was determined from the profile of the droplets. Discs were prepared by compression under controlled conditions: 300 mg of the sample and a pressure of 10^7 Pa, in a typical IR die. The water contact angle was measured within 5 s after full separation from the syringe needle tip.

The thermal decomposition measurements were performed by the thermogravimetric analysis (TA instrument, TGA Q5000, USA). The samples were dried isothermally at 60 °C for 20 min before heating from 60 to 1000 °C at a heating rate of 10 °C min^{-1} under air atmosphere. The amount of surfactant adsorbed on the $CaCO_3$ surface was calculated from the ash content percentage for the $CaCO_3$ samples at 500 °C, which was chosen because it is the temperature at which the surfactant on the $CaCO_3$ surface completely decomposed while the decarbonation of the $CaCO_3$ did not start yet.

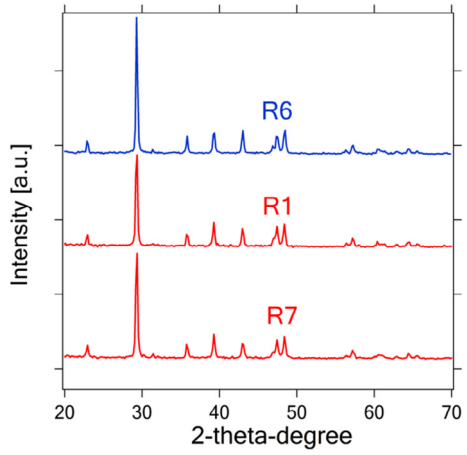

Figure 1 XRD patterns of the prepared calcites: (R6) unmodified, (R1) 2 wt% oleate modified, and (R7) 4 wt% oleate modified.

The zeta potential of $CaCO_3$ particles in suspension was measured at 25 °C using a zeta meter 3.0 equipped with a microprocessor unit (Malvern Instrument Zetasizer 2000). The prepared samples contained 1 mg of $CaCO_3$ dispersed in 100 g monodistilled water. The samples were treated by ultrasonic-horn for 30 min and magnetically stirred for 10 min. The unit automatically calculates the electrophoretic mobility of the particle and converts it into zeta potential using the Smoluchowski equation.

3. Results

3.1. Polymorph and crystallite size

X-ray diffraction patterns of the unmodified (R6) and oleate-modified $CaCO_3$ (R1, R7) are represented in Fig. 1. XRD results show that all the prepared samples exhibit the characteristic reflection of rhombohedral calcite. XRD results indicate that the overall crystalline structure and phase purity of the $CaCO_3$ particles were obtained. All the relatively sharp peaks are indexed to the typical calcite phase of $CaCO_3$ (JCPDS 88-1808). No characteristic peaks of other impurities were observed, which indicated that the products have high purity (Bala et al., 2006). The effects of CaO concentration, CO_2 gas flow rate and sodium oleate concentration on the crystallite size were determined and represented in Figs. 2 and 3 and Table 2. The statistical calculation of this study shows that the average crystal size ranges between 48 and 101 nm. The standard deviation (6.0) and the determination coefficient R^2 (0.9081) indicate the agreement of the generated model with the experimental results. The regression Eq. (3) shows the dependence of the response on the process parameters. The parameters of the equation were obtained by multiple regression analysis of the experimental data.

$$\text{Crystal size nm} = +66.99 + 13.89 * A - 1.35 * B - 2.74 * C - 5.31 * B^2 - 3.65 * A * B - 10.02 * A * C - 9.10 * B * C \quad (3)$$

where,

A = CaO concentration, M;
B = CO_2 flow rate, mL min^{-1};
C = surfactant concentration, %.

The data extracted from the simulation in Figs. 2 and 3 show that the CaO and surfactant concentration are the most significant factors affecting the crystal size of $CaCO_3$. For example without adding surfactant, the crystal size is predicted to increase approximately from 35 to 91 nm with increasing CaO concentration (0.2 → 0.9 M) and CO_2 flow rate (150 → 370 mL min^{-1}) (Fig. 2a). Upon addition of 2 wt% sodium oleate the crystallite size increases approximately from 49 to 77 nm with increasing CaO concentration (0.2 → 0.9 M) and CO_2 flow rate (150 → 290 mL min^{-1}) (Fig. 2b). Upon addition of 4 wt% sodium oleate the crystallite size decreases

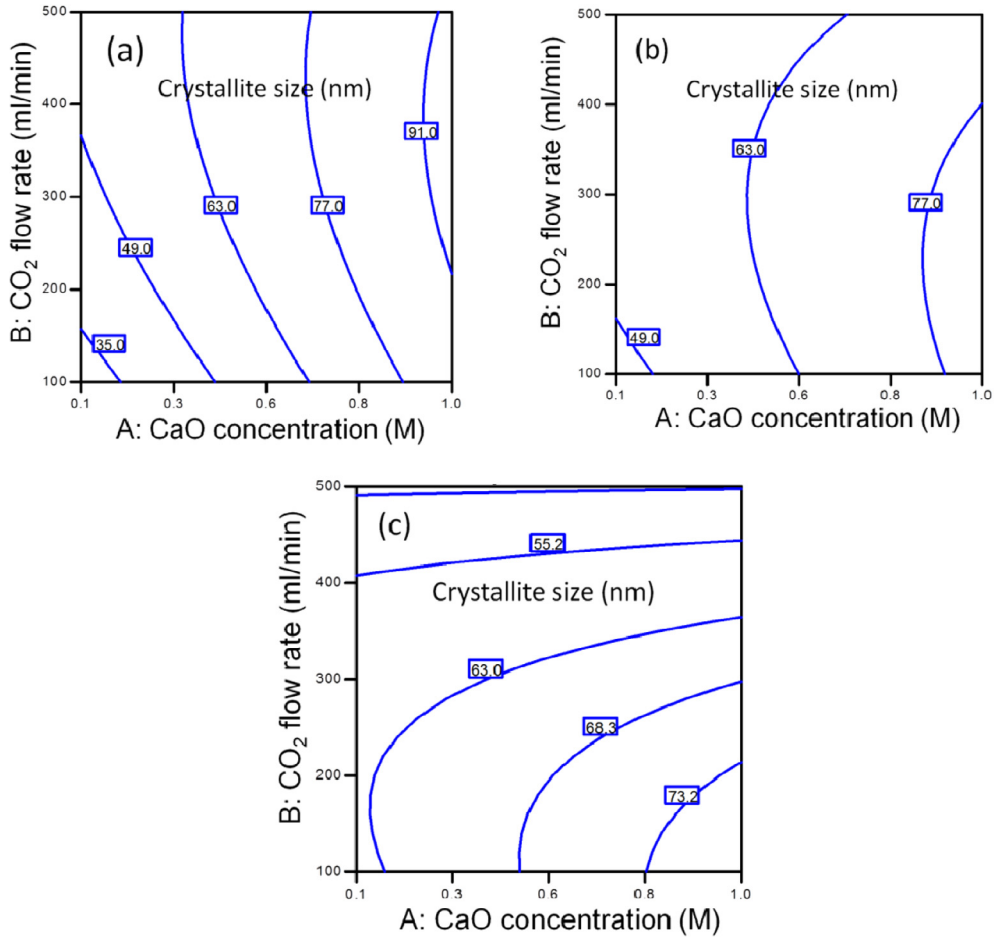

Figure 2 Contour plots for the effects of CaO concentration, CO_2 flow rate, surfactant concentration; (a) 0 wt%; (b) 2 wt%; (c) 4 wt% sodium oleate. Standard deviation: 6.0; R^2: 0.9081.

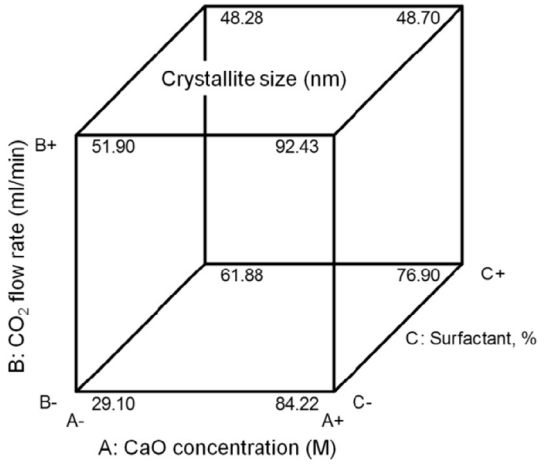

Figure 3 Contour plot (cubic graph) for the effects of CaO concentration, CO_2 flow rate, surfactant concentration. Standard deviation: 6.0; R^2: 0.9081.

approximately from 63 to 55 nm with increasing CaO concentration ($0.4 \rightarrow 0.6$ M) and increasing CO_2 flow rate ($300 \rightarrow 450$ mL min^{-1}) (Fig. 2c). The differences in particle size become even small when using 4 wt% of surfactant and for high flow rates above 300 mL min^{-1} the concentration does no longer influence the particle size. This is obvious from the almost horizontal contour lines for a surfactant concentration of 4 wt% (Fig. 2c) compared to almost vertical contour lines in the absence of surfactant (Fig. 2a). These results can also be retrieved in the 3-D cubic plot (Fig. 3). The data collected at the 3-D cubic reveal that the largest crystallite size, 92 nm can be obtained at high levels of CaO concentration, CO_2 flow rate and absence of the surfactant, which is consistent with the experimental findings. On the other hand, according to the prediction of the model, the smallest crystallite size, 29.1 nm can be achieved only at the lowest levels of CaO concentration, low CO_2 flow rate and absence of the sodium oleate. Comparing the experimental results with the model it was observed that the CaO concentration is the most significant factor affecting the crystallite and particle size of $CaCO_3$. At high CaO concentrations (1 M) the effect of the surfactant and CO_2 flow rate is significant and the differences in crystallite sizes were quite large. When the CaO concentration decreases to 0.1 M, the model deviates somewhat from the experimental results. This can in part be due to the fact that at very low CaO concentration (0.1 M) the effect of the surfactant concentration and CO_2 flow rate is limited and the differences in crystallite sizes are not very large (Table 2, see R1, R3, R5 and R7).

Table 2 Experimental condition of the prepared calcites versus the crystallite size.

Run no.	CaO conc. (M)	CO_2 flow rate (ml min^{-1})	Surf. conc. (wt SO/wt $CaCO_3$)	Crystallite size (nm)
R1	0.1	100	2	49.5
R2	1	100	2	79.4
R3	0.1	500	2	53.6
R4	1	500	2	68.9
R5	0.1	300	0	48.4
R6	1	300	0	101.4
R7	0.1	300	4	53.3
R8	1	300	4	66.2
R9	0.55	100	0	50.4
R10	0.55	500	0	66.4
R11	0.55	100	4	72.8
R12	0.55	500	4	52.4
R13	0.55	300	2	66.6
R14	0.55	300	2	66.6
R15	0.55	300	2	66.6

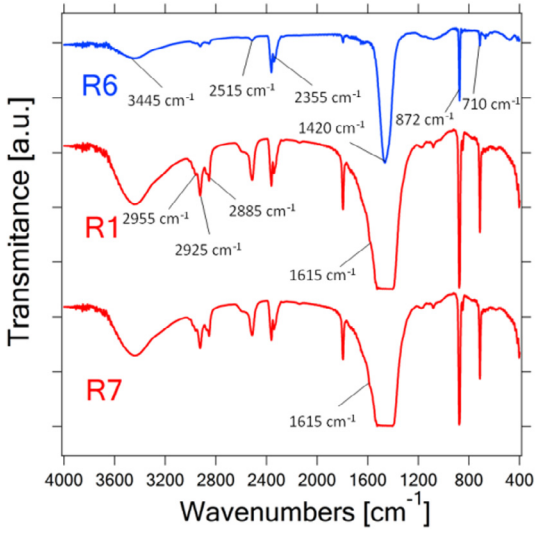

Figure 4 FT-IR spectra of the prepared calcites: (R6) unmodified, (R1) 2 wt% oleate modified, and (R7) 4 wt% oleate modified.

3.2. Fourier transform infrared spectroscopy

FT-IR spectra of the unmodified (R6) and oleate-modified $CaCO_3$ (R1, R7) are shown in Fig. 4. The characteristic absorption peaks of calcite $CaCO_3$ are stretching vibrations of the C–O approximately at 1420 cm^{-1} and bending vibrations of the C–O approximately at 872 and 710 cm^{-1}. The combination of the three peaks at 1420, 872 and 710 cm^{-1} appears at 2515 cm^{-1}, and is called overtone or combination band (Forbes et al., 2011). The broad absorption peaks around 3445 cm^{-1} are assigned to stretching vibrations of the O–H bond and it can be attributed to the presence of absorbed water and hydroxyl groups on the surface of $CaCO_3$ particles. The peaks around 2355 cm^{-1} are attributed to carbon dioxide in the atmosphere.

Comparing with the literature (Forbes et al., 2011) the characteristic IR spectra indicate that all the prepared samples are typically calcite crystals. Comparing the unmodified and oleate-modified samples, a shoulder at 1615 cm^{-1} and peaks at 2955, 2925 and 2885 cm^{-1}, are observed for oleate-modified $CaCO_3$. The shoulder at 1615 cm^{-1} corresponds to the appearance of a carboxylic salt, indicating that oleate has been attached to the surface of $CaCO_3$. The peaks at 2955, 2925 and 2885 cm^{-1}, are ascribed to the C–H stretching of the long alkyl chain of oleate and prove the presence of oleate at the surface of $CaCO_3$. The XRD along with FT-IR results show that no other crystalline phases such as aragonite and vaterite were detected (Vagenas et al., 2003). Sodium oleate has no significant effect on the $CaCO_3$ polymorph.

3.3. Particle size and morphology

Fig. 5 shows TEM images of oleate-modified (R1, R7) and unmodified (R6) $CaCO_3$. The results show that the use of

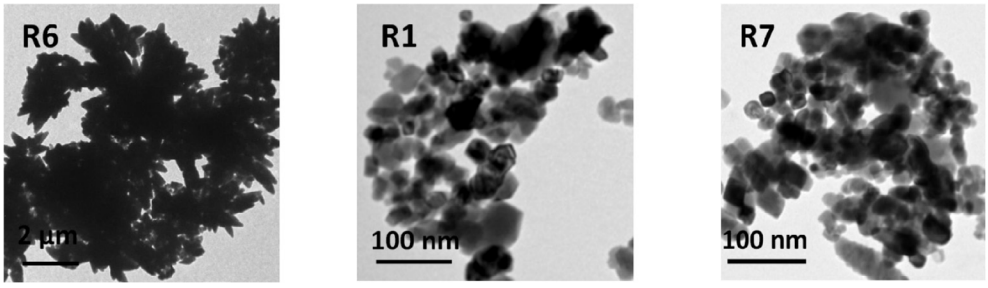

Figure 5 TEM images of the prepared calcites: (R6) unmodified, (R1) 2 wt% oleate modified, and (R7) 4 wt% oleate modified.

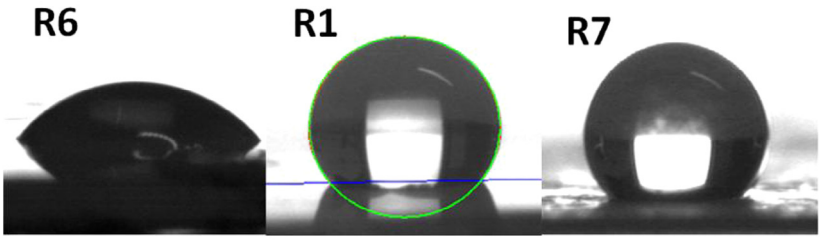

Figure 6 Water contact angle of the prepared calcites: (R6) unmodified, (R1) 2 wt% oleate modified, and (R7) 4 wt% oleate modified.

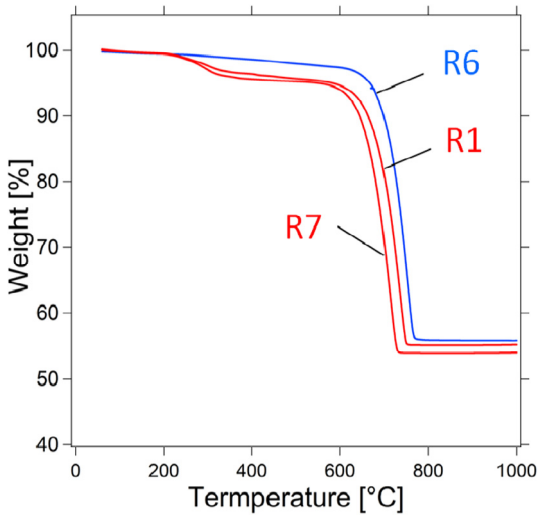

Figure 7 TGA curves of the prepared calcites: (R6) unmodified, (R1) 2 wt% oleate modified, and (R7) 4 wt% oleate modified.

1 M CaO concentration and 300 mL min^{-1} forms 1–1.5 μm length scalenohedral particles. The size and morphology of $CaCO_3$ is changed from 1–1.5 μm length scalenohedral particles to 20–40 nm rhombohedral particles upon addition of 2 wt% or 4 wt% sodium oleate. This indicates that addition of sodium oleate can significantly inhibit the crystal and particle growth of $CaCO_3$. Increasing the sodium oleate concentration from 2 wt% to 4 wt% has no significant effect on the size and morphology of $CaCO_3$.

3.4. Surface properties

The average water contact angle (WCA) of unmodified $CaCO_3$ (R6) is approximately 25°. Upon addition of 2 wt% and 4 wt% sodium oleate the average water contact angle (WCA) increases to 127° and 129°, respectively (Fig. 6). Within 15 s, the water droplet on the unmodified $CaCO_3$ powder disc (R6) is completely absorbed while the droplets on the oleate modified discs (R1 and R7) are absorbed much slower and the contact angle decreases from 129° and 127° to about 90° which can also be observed from water contact angle measurements as explained by Hu and Deng, 2010.

Fig. 7 shows the thermal decomposition curves of the unmodified (R6) and oleate-modified (R1, R7) $CaCO_3$. From the weight loss curve of the unmodified $CaCO_3$ (i.e. R6) it was observed that the weight loss happens in two steps from 60 to 500 °C and from 500 to 1000 °C. The mass loss of 0.35–0.55 wt% from 60 to 190 °C is probably due to desorption of the physically adsorbed water. The mass loss of 1.2–2 wt% from 200 to 500 °C is probably due to desorption of the structural water. The data extracted from Fig. 7 show that the amount of adsorbed oleate for the oleate modified $CaCO_3$ R1 (modified 2 wt% sodium oleate) reaches up to 1.7 wt% and for R7 (modified 4 wt% sodium oleate) it reaches to 2.2 wt% compared with the unmodified $CaCO_3$ which shows weight loss between 60 and 500 °C due to loss of physically and chemically sorbed water. Mass loss measurements prove that oleate can effectively be adsorbed on the $CaCO_3$ surface. The zeta potential of the unmodified $CaCO_3$ (R6) is approximately −15 mV at pH 9. The zeta potential of $CaCO_3$ decreases to a more negative potential of −22 mV namely −26 mV with addition of 2 wt% and 4 wt% sodium oleate.

4. Discussion

The preparation variables, CaO concentration, CO_2 gas flow and surfactant concentration, affect the growth rates of different crystal faces of $CaCO_3$ during its growth and hence they affect the crystallite size, particle size and morphology of $CaCO_3$. In the absence of sodium oleate, the use of a high CaO concentration and low CO_2 flow rate microsize particles are formed that are composed of rather big crystallites approximately 101 nm in diameter. The excess of Ca^{2+} in the bulk solution and a low CO_2 flow rate elongate the reaction and growth time of the precipitated crystals/particles and lead to the observed increase of the crystallite and particle size. These results are consistent with the literature (García Carmona et al., 2003).

Upon addition of sodium oleate, the oleate's carboxylic groups (–COO^-) complexate the Ca^{2+} ions on the crystal surface and inhibit the crystal/particle growth. Meanwhile, the hydrophobic tails pointing outwards change the surface characteristics of $CaCO_3$ particles, from hydrophilic to hydrophobic. In addition, the oleate ions can be situated at the gas–liquid interface. Consequently, they increase the stability of CO_2 bubbles and prevent their aggregation (García Carmona et al., 2003; Sun and Deng, 2004). Maintenance of CO_2 bubbles in the solution accelerates the dissolution of CO_2 gas and increases the CO_3^{2-}:Ca^{2+} ionic ratio and the nucleation rate and leads to the decrease of particle/crystallite size. The suggested mechanism can be confirmed by XRD, FT-IR, HRTEM, water contact angle, zeta potential and TGA measurements, see Figs. 1–6. The carbonation mechanism of lime particles in the presence of fatty acid surfactant (R–COONa) can be represented by Eqs. (4)–(7):Hydration of lime CaO:

$$CaO_{(S)} + H_2O_{(aq)} \rightarrow Ca^{2+}_{(aq)} + 2OH^{-}_{(aq)} \quad (4)$$

Dissociation/association of surfactant:

$$R\text{–}COONa_{(S)} \rightarrow R\text{–}COO^{-}_{(aq)} + Na^{+}_{(aq)} \quad (5)$$

$$2R\text{–}COO^{-}_{(aq)} + Ca^{2+}_{(aq)} \rightarrow (R\text{–}COO)_2Ca_{(aq)} \quad (6)$$

$$Ca(OH)_{2(S)} + (R\text{–}COO)_2Ca_{(aq)} \rightarrow Ca(OH)_{2(S)} - Ca(R\text{–}COO)_2 \quad (7)$$

Partial dissolution of CO_2 gas:

$$CO_{2(g)} + H_2O_{(aq)} \rightarrow 2H_2O_{(aq)} + CO^{-}_{3(aq)} \quad (8)$$

Carbonation of lime solution:

$$Ca(OH)_{2(S)}\text{---}Ca(OOC\text{–}R)_2 + CO^{-}_{3(aq)} \rightarrow CaCO_{3(S)}\text{---}Ca(OOC\text{–}R)_2 \quad (9)$$

When the crystals are immersed in an electrolytic solution, whether it is in a thermodynamic equilibrium or not, some exchanges are possible between the crystal lattice ions and the ions in solution, even if these ions are of comparable size or not. This induces some modifications of crystal composition dependent on the adsorption of foreign ions present in solution or on preferential "scrubbings" of some crystal lattice ions (Moulin and Roques, 2003). In the case of oleate modified $CaCO_3$ (R1, R7), adsorption of the oleate on the surface $CaCO_3$ alternates the surface composition of these crystals and reduces the surface potential of $CaCO_3$ to more negative values.

5. Conclusion

Superhydrophobic nanocalcite crystals were successfully prepared via bubbling carbonation of the CaO–CO_2–H_2O system with a surfactant (sodium oleate). Statistically designed experiments based on Box–Behnken procedure were used to study the effects of three variables, CaO concentration, CO_2 flow rate and surfactant concentration on the crystallite size of $CaCO_3$ particles. Experimental results show that calcite crystals of average crystal sizes ranging between 48 and 101 nm were successfully produced. According to the simulation the CaO concentration is the most significant factor affecting the crystallite size of $CaCO_3$ especially in the absence of the surfactant. At low CaO concentration the effect of CO_2 flow rate and surfactant concentration is limited. Sodium oleate plays a significant role during the preparation of $CaCO_3$. The oleate's carboxylic groups ($-COO^-$) are able to bind effectively to the Ca^{2+} ions on the crystal surface and efficiently inhibit the crystal/particle growth. Addition of 0–4 wt% sodium oleate helps in inhibiting the crystal and particle growth of $CaCO_3$ and it changes the surface characteristics of $CaCO_3$ from highly hydrophilic to superhydrophobic. Addition of 4 wt% even reduces the influence of the CaO concentration on the particle size.

Acknowledgments

This work was partially supported by the Egyptian Science and Technology Development Fund (STDF) under Grant No. ID 737. A.B. would like to thank Prof. Yulin Deng (School of Chemical and Biomolecular Engineering, Georgia Institute of Technology) for his help and valuable discussions.

References

Avella, M., Errico, M.E., Martuscelli, E., 2001. Novel PMMA/$CaCO_3$ nanocomposites abrasion resistant prepared by an in situ polymerization process. Nano Lett. 1, 213–217.

Bala, H., Ding, X., Guo, Y., Deng, Y., Wang, C., 2006. Multigram scale synthesis and characterization of monodispersed cubic calcium carbonate nanoparticles. Mater. Lett. 60, 1515–1518.

Barhoum, A., Rahier, H., Esmail Abou-Zaied, R., Rehan, M., Dufour, T., Hill, G., Dufresne, A., 2014. Effect of cationic and anionic surfactants on the application of calcium carbonate nanoparticles in paper coating. ACS Appl. Mater. Interfaces 6, 2734–2744.

Brecevic, L., Kralj, D., 2007. On calcium carbonates: from fundamental research to application. Croat. Chem. Acta 80, 467–484.

Di Lorenzo, M.L., Errico, M.E., Avella, M., 2002. Thermal and morphological characterization of poly(ethylene terephthalate)/calcium carbonate nanocomposites. J. Mater. Sci. 37, 2351–2358.

El-Sheikh, S.M., El-Sherbiny, S., Barhoum, A., Deng, Y., 2013. Effects of cationic surfactant during the precipitation of calcium carbonate nano-particles on their size, morphology, and other characteristics. Colloids Surf. A 422, 44–49.

Forbes, T.Z., Radha, A.V., Navrotsky, A., 2011. The energetics of nanophase calcite. Geochim. Cosmochim. Acta 75, 7893–7905.

García Carmona, J., Morales, J.G., Clemente, R.R., 2003. Rhombohedral–scalenohedral calcite transition produced by adjusting the solution electrical conductivity in the system of $Ca(OH)_2$–CO_2–H_2O. J. Colloid Interface Sci. 261, 434–440.

Hu, Z., Deng, Y., 2010. Superhydrophobic surface fabricated from fatty acid-modified precipitated calcium carbonate. Ind. Eng. Chem. Res. 49, 5625–5630.

Ihli, J., Wong, W.C., Noel, E.H., Kim, Y.Y., Kulak, A.N., Christenson, H.K., Duer, M.J., Meldrum, F.C., 2014. Dehydration and crystallization of amorphous calcium carbonate in solution and in air. Nat. Commun. 5, 1–10.

Lanzon, M., Garrido, A., Garcia-Ruiz, P.A., 2011. Stabilization of sodium oleate as calcium oleate in cement-based mortars made with limestone fillers. Constr. Build. Mater. 25, 1001–1008.

Liang, J.Z., Zhou, L., Tang, C.Y., Tsui, C.P., 2013. Crystallization properties of polycaprolactone composites filled with nanometer calcium carbonate. J. Appl. Polym. Sci. 128, 2940–2944.

Moulin, P., Roques, H., 2003. Zeta potential measurement of calcium carbonate. J. Colloid Interface Sci. 261, 115–126.

Michaux, F., Carteret, C., Stébé, M.J., Blin, J.L., 2013. Investigation of properties of mesoporous silica materials based on nonionic fluorinated surfactant using Box–Behnken experimental designs. Micropor. Mesopor. Mater. 174, 135–143.

Reeder, R.J., Tang, Y.Z., Schmidt, M.P., Kubista, L.M., Cowan, D.F., Phillips, B.L., 2013. Characterization of structure in biogenic amorphous calcium carbonate: pair distribution function and nuclear magnetic resonance studies of lobster gastrolith. Cryst. Growth Des. 13, 1905–1914.

Rodriguez-Blanco, J.D., Shaw, S., Benning, L.G., 2011. The kinetics and mechanisms of amorphous calcium carbonate (ACC) crystallization to calcite, via vaterite. Nanoscale 3, 265–271.

Sheng, Y., Zhou, B., Wang, C.Y., Zhao, X., Deng, Y.H., Wang, Z.C., 2006. In situ preparation of hydrophobic $CaCO_3$ in the presence of sodium oleate. Appl. Surf. Sci. 253, 1983–1987.

Sun, Q.H., Deng, Y.L., 2004. Effect of various factors on the particle size of calcium carbonate formed in a precipitation process. J. Colloid Interface Sci. 278, 170–179.

Tomioka, T., Fuji, M., Takahashi, M., Takai, C., Utsuno, M., 2012. Hollow structure formation mechanism of calcium carbonate particles synthesized by the CO_2 bubbling method. Cryst. Growth Des. 12, 771–776.

Ukrainczyk, M., Kontrec, J., Babic-Ivancic, V., Brecevic, L., Kralj, D., 2007. Experimental design approach to calcium carbonate precipitation in a semicontinuous process. Powder Technol. 171, 192–199.

Ukrainczyk, M., Kontrec, J., Kralj, D., 2009. Precipitation of different calcite crystal morphologies in the presence of sodium stearate. J. Colloid Interface Sci. 329, 89–96.

Vagenas, N.V., Gatsouli, A., Kontoyannis, C.G., 2003. Quantitative analysis of synthetic calcium carbonate polymorphs using FT-IR spectroscopy. Talanta 59, 831–836.

Wang, C.Y., Piao, C., Zhai, X.L., Hickman, F.N., Li, J., 2010. Synthesis and character of super-hydrophobic $CaCO_3$ powder in situ. Powder Technol. 200, 84–86.

Wen, Y., Xiang, L., Jin, Y., 2010. Synthesis of plate-like calcium carbonate via carbonation route. Mater. Lett. 57, 2565–2571.

Wu, G.H., Wang, Y.J., Zhu, S.L., Wang, J.D., 2007. Preparation of ultrafine calcium carbonate particles with micropore dispersion method. Powder Technol. 172, 82–88.

Zaky, R.R., Hessien, M.M., El-Midany, A.A., Khedr, M.H., Abdel-Aal, E.A., El-Barawy, K.A., 2008. Preparation of silica nanoparticles from semi-burned rice straw ash. Powder Technol. 185, 31–35.